Gate-tunable non-volatile photomemory effect in MoS_2 transistors

Andreij C. Gadelha,[1] Alisson R. Cadore,[1] Kenji Watanabe,[2] Takashi Taniguchi,[2] Ana M. de Paula,[1] Leandro M. Malard,[1] Rodrigo G. Lacerda,[1] and Leonardo C. Campos[1]

[1]*Departamento de Fisica, Universidade Federal de*
Minas Gerais, Belo Horizonte, MG 31270-901, Brazil

[2]*Advanced Materials Laboratory, National Institute for*
Materials Science, 1-1 Namiki, Tsukuba 305-0044, Japan

Abstract

Non-volatile memory devices have been limited to flash architectures that are complex devices. Here, we present a unique photomemory effect in MoS_2 transistors. The photomemory is based on a photodoping effect - a controlled way of manipulating the density of free charges in monolayer MoS_2 using a combination of laser exposure and gate voltage application. The photodoping promotes changes on the conductance of MoS_2 leading to photomemory states with high memory on/off ratio. Such memory states are non-volatile with an expectation of retaining up to 50% of the information for tens of years. Furthermore, we show that the photodoping is gate-tunable, enabling control of the recorded memory states. Finally, we propose a model to explain the photodoping, and we provide experimental evidence supporting such a phenomenon. In summary, our work includes the MoS_2 phototransistors in the non-volatile memory devices and expands the possibilities of memory application beyond conventional memory architectures.

Introduction

Due to the ultra-thin nature and tunable electrostatic properties of two-dimensional (2D) materials, they have strategical importance for digital electronics and memory applications. The required features (figures of merit) for actual memory devices include the miniaturisation capability, the power consumption (high memory on/off ratio), the operation speed, the memory retention time and the cost. Innately, the 2D materials based devices show advantages for miniaturization, however to date there are no reported simple memory devices that cover most of the required features, notably the memory retention time [1–17]. Monolayer MoS_2 is a direct band gap 2D semiconductor material [18, 19] that shows high photocurrent response [20–25], high photoluminescence emission [26, 27] and interesting valleytronic properties [28–31]. Thus, MoS_2 based flash memory devices with high memory on/off ratio and long memory retention time have emerged. However, the implementation of flash devices is challenging because they require engineering with many elements into complex architectures. More recently, floating-gate tunneling devices using simpler architechtures than flash devices have been proposed but they lack ultrahigh time-stability [15–17]. Therefore, the development of alternative, high-performance, simpler memory architectures is strategical. Toward this direction, some reports have investigated a thermally assisted memory effect [6] and an optical memory effect [5] in a MoS_2 field effect transistor (FET) that is also a simpler architecture than flash devices. Nonetheless, in the first case, the memory effect has a drawback of not operating at room temperature and both cases [5, 6] showed low memory on/off ratio and short memory retention time.

Here we show that we can obtain a non-volatile photomemory effect with high on/off ratio in a MoS_2 FET architecture. Such photomemory effect is based on a photodoping process that changes the MoS_2 conductance in a way that promotes two distinguishable binary photomemory states with on/off ratio up to 10^6. The photogenerated memory states are persistent and predicted to retain up to 50% of its information for decades, that leads to a non-volatile photomemory. Moreover, it is important to mention that the presented photomemory is gate-tunable. The gate voltage is used to both adjust the memory on/off ratio (with the laser off) and to manipulate the recorded photomemory states during the laser exposure. Finally, we explore and discuss a possible physical mechanism of the photodoping that is also supported by our experimental evidence. In summary, we propose a pho-

tomemory effect in MoS_2 FETs that expands the possibilities of memory application beyond conventional memory architectures.

Results and Discussion

The photomemory effect investigated in this work is due to the modulation of the conductance of a monolayer MoS_2 field effect transistor via a simultaneous application of light and electrostatic gate potential. Along this paper, we show evidence that the main mechanisms for the photomemory relies on the manipulation of a charging effect at the gate-insulator interface of the FET (the interface between the insulator and the material of the gate terminal). Although other mechanisms can have some influence on the photomemory, we show that our model explains well our results. Our FET is a Van der Waals heterostructure consisting of a monolayer MoS_2 supported by a high-quality hexagonal Boron Nitride crystal (BN), see Fig. 1(a). In this case, we use a graphite crystal to provide a flat back gate electrode. In Fig. 1(b) we present an atomic force spectroscopy (AFM) phase image of one of the devices measured in this work. While, in the Supplementary Information we depict the characterization for the second device.

We start by presenting the process of photocurrent generation in the MoS_2 FET. Fig. 1(c) shows a typical time-resolved photocurrent measurement of our device. Initially we measure the standard current (I_{SD}) in dark conditions, then we illuminate the device using the laser ($\lambda = 488\,\text{nm}$) for 20 s and $V_{BG} = -5\,\text{V}$. We use the same laser with $\lambda = 488\,\text{nm}$ for all the optoelectronic measurements that we present in this text. A careful analysis of the current as a function of time reveals that there are two optical processes generating the photocurrent in the MoS_2 channel. First, we observe a rapid increase of I_{SD} due to excitation of electron-hole pairs (see vertical black arrow), then a second and slow process that dominates the photocurrent. We observe the same trend when the laser is turned off. There is a rapid collapse of I_{SD}, due to the recombination of electron-hole pairs, then a prolonged decay process that leads to a persistent photocurrent (PPC). The photodoping effect causes the PPC. We will discuss this process later. For now, we will define the photomemory states "ON" and "OFF". In Fig. 1(c) we ascribe the PPC as the "ON" state, while the current before the laser exposure is the "OFF" state, which are binary photomemory states.

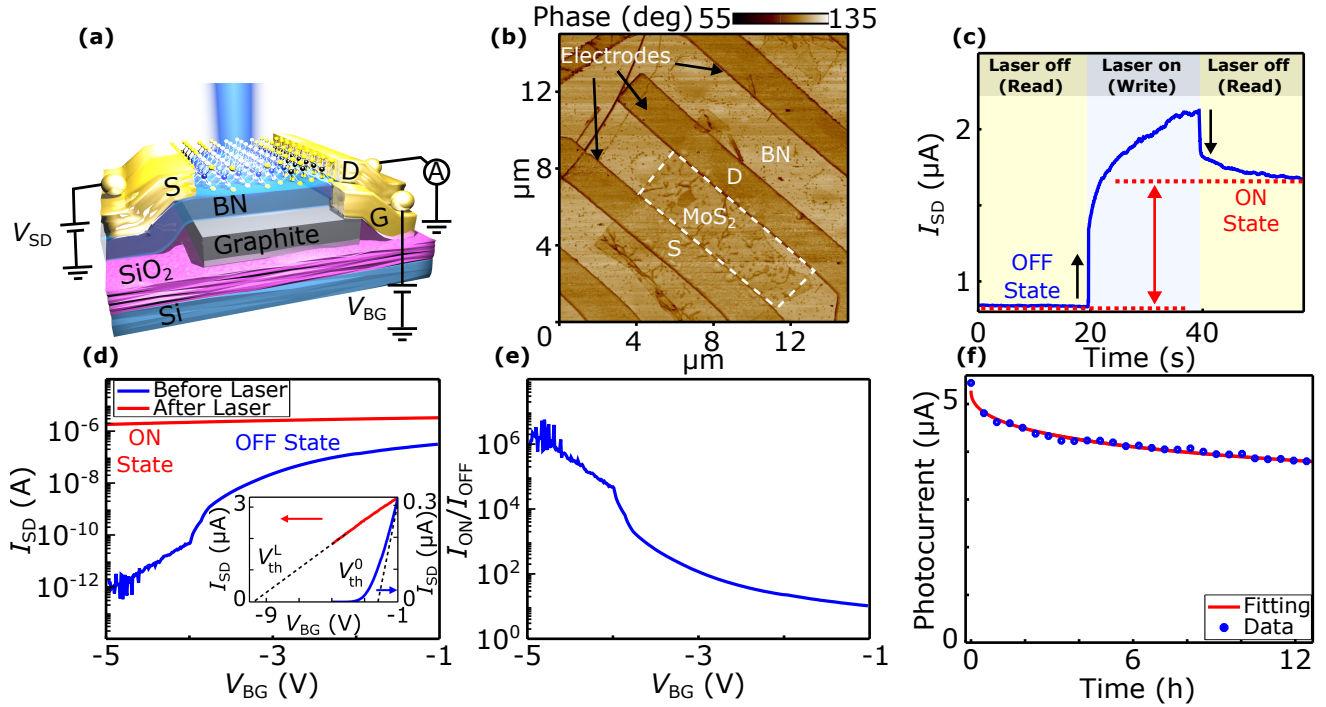The photomemory effect is better observed in Fig. 1(d), where we show the transfer

3

FIG. 1. **Photodoping and non-volatile photomemory**. **(a)**, sketch of the MoS$_2$ FET. **(b)**, AFM phase image of the device. **(c)**, time resolved photocurrent, laser exposure at 488 nm with fluence of 60 μW/μm^2. The parameters are $V_{BG} = -5$ V and $V_{SD} = 0.1$ V. **(d)**, The I_{SD} vs V_{BG} measurements on a log scale before (blue) and after (red) the laser exposure, $V_{SD} = 0.1$ V. In the inset, the same measurements but on a linear scale. The red curve is measured after the 488 nm laser exposure with fluence of 700 μW/μm^2 and $V_{BG} = -5$ V until photocurrent saturation. **(e)**, I_{ON}/I_{OFF} ratio as a function of the gate voltage. **(f)**, photocurrent decay after the photodoping induced by the 488 nm laser with fluence of 700 μW/μm^2 until photocurrent saturation. The parameters $V_{BG} = 0$ V and $V_{SD} = 0.1$ V are used for this measurement.

curves, I_{SD} vs back gate voltage (V_{BG}) curves, on a log scale. In the inset, we plot the the same curves, but on a linear scale. In blue, we plot a transfer curve before the laser exposure. By extrapolating the I_{SD} curve we estimate the threshold voltage (V_{th}) as $V_{th}^0 = -2.2$ V, see the inset in Fig. 1(d). After this, the MoS$_2$ device is exposed to the laser beam with $V_{BG} = -5$ V until the photocurrent saturates. The reason for waiting the photocurrent saturation is to reach the best response of our device. Then, we turn the laser off and repeat the transfer curve measurement. The data from the transfer curve after the laser exposure (red curve in Fig. 1(d)) displays a significant increase of I_{SD} at all applied gate conditions.

4

It is important to note that there is a shift of V_{th} towards V_{BG} out of the range of the experiment. This shift is a signature of a photodoping effect. It means that the density of free charges of MoS_2 has changed after the laser exposure. We estimate by extrapolating the data that the initial $V_{\mathrm{th}}^0 = -2.2\,\mathrm{V}$ shifts to $V_{\mathrm{th}}^{\mathrm{L}} = -9.8\,\mathrm{V}$, see the inset in Fig. 1(d). Also, the expected change in the density of charge of the MoS_2 due to photodoping is $\Delta n_{\mathrm{ph}} = 6 \times 10^{12}\,\mathrm{cm}^{-2}$. Which is evaluated using the equation:

$$\Delta n_{\mathrm{ph}} = \frac{\varepsilon_0 \varepsilon_{ox}}{e\,d}(V_{\mathrm{th}}^{\mathrm{L}} - V_{\mathrm{th}}^0) \tag{1}$$

where $\varepsilon_{\mathrm{ox}}$ and d are the dielectric constant of the insulator and its thickness, respectively. Note that such extra doping is obtained simply by the combination of the laser exposure and the applied gate bias.

We now describe the methods used here to define the photomemory states, that can also be used to perform the "read" operations. We consider as an "OFF" state the measured I_{SD} before the laser exposure for a given V_{BG} (no information is recorded in the photomemory), see the blue curve in Fig. 1(d). Similarly, the measured I_{SD} after the laser exposure for the same V_{BG} is considered as an "ON" state, see the red curve Fig. 1(d). Another method to determine, or to "read", the photomemory states is by measuring Δn_{ph} before and after the laser exposure. We reinforce that we perform the "read" operations with the laser off. We will discuss the "record" operations later, which are the procedures that "write" and "erase" the memory states. Because I_{SD} is a function of V_{BG}, by measuring I_{SD} instead of Δn_{ph} we have the advantage to use the gate voltage (with the laser off) to optimise the gain of the photomemory [1, 32]. We elucidate this fact in Fig. 1(e), where we plot the $I_{\mathrm{ON}}/I_{\mathrm{OFF}}$ ratio (memory on/off ratio) as function of V_{BG}. The $I_{\mathrm{ON}}/I_{\mathrm{OFF}}$ ratio changes from 10, for positive gate voltages, to values up to 10^6, for negative gate voltages. Observe that the high modulation of the memory on/off ratio with gate voltage is an attribute of the photomemory effect. It must be noted that to reach the photocurrent saturation we do exposures of 30 min, for example in Fig. 1(d). However, we can also obtain a high memory on/off ratio of 10^4 with a short exposure time (20 s), see Fig. S14.

Another crucial figure of merit of a memory device is the memory retention time. To assess that, we measure the MoS_2 photocurrent decay over time, applying $V_{\mathrm{SD}} = 0.1\,\mathrm{V}$ and $V_{\mathrm{BG}} = 0\,\mathrm{V}$, see the blue dots in Fig. 1(f). We measure the decay after the photocurrent saturation by the laser exposure. After $15\,\mathrm{h}$ the photocurrent barely decreases, suggesting

that the photomemory state is permanent. So, the photomemory is a non-volatile memory. To estimate the memory loss over ten years, we employ an exponential decay fit, the red line in Fig. 1(f). From the fitting, we predict that the reminiscent memory current for the photomemory device is approximately 50% of the initial photocurrent. Thus, the devices can retain 50% of the memory for ten years. These values are much better than the ones for the MoS_2 flash memory architectures, where the retention percentage is in the range of 15-30% [1–4].

We can now describe in more details the photomemory device, which is composed mainly of two elements in the FET architecture. One element is the gate-insulator interface, where possibly the charges are trapped inducing the photodoping. The other element is the semi-conductor channel, from which we "read" the photomemory states. In this way, we can design better photomemory devices by choosing other gate-insulator interfaces that can provide higher values of photodoping and retention time. Furthermore, the choices of semi-conductors with better mobility and subthreshold swing would enable to achieve higher on/off ratio values.

The photomemory achieved on a FET architecture has the advantage that we can improve some features by choosing the adequate gate voltages. One example is the high memory on/off ratio already discussed. Another important feature is that we can select distinguishable photomemory states for the same laser exposure due to the photodoping dependence on the gate voltage. In this way, the gate voltage is used both to "read" and to "record" the photomemory states. Here, we define of "record" operation the procedure of doing in our devices laser exposures concomitantly with the gate voltage application. In Fig. 2 we show results that highlight the "recording" of the photomemory states. Fig. 2(a) reveals the changes in the density of free charges due to the photodoping effect by exhibiting multiple transfer curves at different photomemory states. The blue curve represents the "OFF" state before any laser exposure. After the "OFF" state is measured, by evaluating a transfer curve of the device, we "record" a photomemory state by applying $V_{BG} = -2\,\mathrm{V}$ and by exposing the photomemory device to the laser for 20 s. After this "record" operation, we measure a new transfer curve with the laser off (black curve in Fig. 2(a)) and from the data of Fig. 2(a) we observe that the MoS_2 sheet acquires a new density of charge after the laser exposure. We evaluate the new density of free charges from the equation 1 as a function of the new V_{th}. To visualise how the transfer curve changes at every "record" operation, the

process described above is repeated applying gate voltages during the "record" operations up to $V_{BG} = -5\,\mathrm{V}$ in steps of $-1\,\mathrm{V}$, as shown in Fig. 2(a). It is interesting to note that for each "record" operation with different V_{BG} there is a distinct transfer curve and thus a particular photomemory state. Then, we can choose several "ON" states with distinct electrical conductivity.
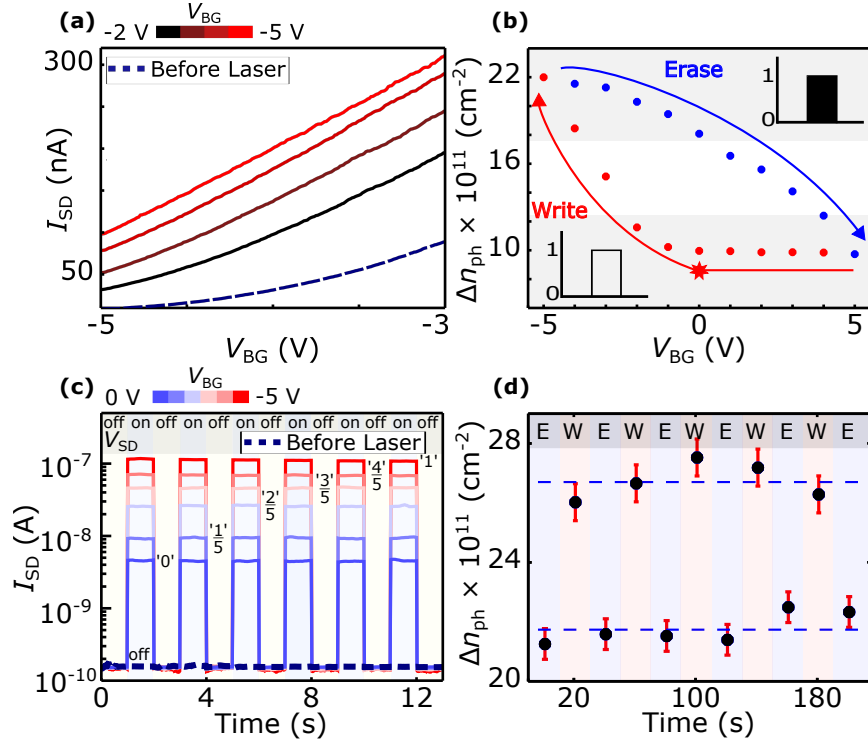

FIG. 2. **Gate-tunable photomemory**. (a), I_{SD} vs V_{BG} curves before laser exposure, blue curve, and after laser exposures with V_{BG} values defined in the color bar. (b), Δn_{ph} vs V_{BG} curve. First the point $V_{BG} = 0\,\mathrm{V}$ is measured and then the arrows indicates the followed applied gate voltages during the laser exposures. For figures (a)-(b) there is a 488 nm laser exposure on each point for 20 s (at laser fluence of 60 $\mu\mathrm{W}/\mu\mathrm{m}^2$). (c), multilevel photomemory, gate values from 0 V to -5 V are used for the "writings" and 20 s of laser exposure at fluence of 700 $\mu\mathrm{W}/\mu\mathrm{m}^2$. For the "readings" a gate value of -4 V and bias pulses of 0.1 V are applied. (d), "write"-"erase" operations, for $V_{BG} = -5\,\mathrm{V}$ and $V_{BG} = 5\,\mathrm{V}$, respectively, and 20 s of laser exposure (fluence of 700 $\mu\mathrm{W}/\mu\mathrm{m}^2$).

Fig. 2(b) exposes the change of the density of free charges acquired for the MoS_2 after every photomemory "record" operation as compared to the intrinsic density of charge of the photomemory (equation 1). Here we use the same "record" operation described in Fig. 2(a), but we achieve the initially recorded state by applying a $V_{BG} = 0\,\mathrm{V}$ during the 20 s

of laser exposure. We name this recorded state as "0" state. We "record" the other photomemory states in the arrows indicated sequence by changing the gate voltages in a range of $-5\,\mathrm{V} \leq V_{\mathrm{BG}} \leq 5\,\mathrm{V}$. The negative gate voltages are used during the "record" operations to monotonically increase the density of charge to set a "1" state and the positive gate voltages are used during the "record" operations to reduce the density of charge and to restore the initial "0" state. We name the process of charge injection in the MoS_2 as a "write" operation (red arrow). We perform the "write" operation by exposing the device to the laser with an applied negative gate voltage. We denominate the process of removing the charges as an "erase" operation (blue arrow). The gate-"erase" operation is performed right after writing the "1" state, but doing "record" operations with gate voltages larger than $V_{\mathrm{BG}} = -5\,\mathrm{V}$. For example, in fig. 2(b) the "erase" operations are executed with several laser exposures applying $V_{\mathrm{BG}} = -4\,\mathrm{V}, -3\,\mathrm{V} \dots 5\,\mathrm{V}$. Also, note that the "erase" operation cannot cancel the photodoping completely, so we still have a reminiscent photodoping of $\Delta n_{\mathrm{ph}} = 10 \times 10^{11}$ after the "erase" operation, see Fig. 2(b).

Fig. 2(b) also shows that the laser "record" operations with different gate voltages generate distinct Δn_{ph} values, which correspond to distinct photomemory states. This dependence of the photomemory states on the V_{BG} used during the "record" operations shows that we can use the photomemory for multilevel "ON" memory states operation. However, we must point out that it is not the aim of this work to explore multilevel memory operation. We only elucidate that the gate-tunability property of photomemory can allow this type of operation. Fig. 2(c) demonstrate how this is possible employing current readings. In Fig. 2(c), the dashed black line represents the "OFF" state, which is measured by applying $V_{\mathrm{SD}} = 0.1\,\mathrm{V}$ and $V_{\mathrm{BG}} = -4\,\mathrm{V}$ before any laser exposure. We "record" "ON" states applying laser exposures using different V_{BG} at each "record" operation. More precisely, we use V_{BG} from 0 V to -5 V, with increments of -1 V, and do laser exposures for 20 s, "recording" multilevel states which we denote by "0", "$\frac{1}{5}$", "$\frac{2}{5}$" ... "1". After each "record" operation, we "read" the photomemory state by measuring the current through the device at the same electrostatic condition used when we "read" the "OFF" state. The difference here is that we use pulses of $V_{\mathrm{SD}} = 0.1\,\mathrm{V}$ for 2 s spaced by 2 s to show that the information is stored in the photomemory even when no V_{SD} is applied. Note that the "OFF" state is shown only for reference and the ratio between ON/OFF states previously discussed does not apply for multilevel operations. However, the gain between such multilevel states can be maximised tuning the

gate-potential, but in our presented data it is of the order of ten.

Although multilevel memory states are interesting, here they are explored only to demonstrate the usefulness of the gate-tunability property of the photomemory. However, for practical memory operations, it is straightforward to explore the reliability in the "write"-"erase" operations between the binary memory states. In this case, we generate the binary "1" and "0" states by applying $V_{\mathrm{BG}} = -5\,\mathrm{V}$ and $V_{\mathrm{BG}} = 5\,\mathrm{V}$, respectively, during the laser exposures of 20 s. We show the reproducibility and reliability of the "write"-"erase" operations of the binary memory states in Fig. 2(d), that presents a sequence of successful "write"-"erase" cycles. These results demonstrate the device robustness. In Fig. 2(d), it is also represented the error bars in each "record" operation. The error bars show that the "write"-"erase" operations generate distinguishable photomemory states.

It is worth mentioning that the variation of the photodoping between the "1" and the "0" states in Fig. 2(b) is $\Delta n_{\mathrm{ph}} \sim 10^{12}\,\mathrm{cm}^{-2}$, which is evaluated by $\Delta n_{\mathrm{ph}} = \frac{\varepsilon_0 \varepsilon_{ox}}{e\,d}(V_{\mathrm{th}}^{\text{“1”}} - V_{\mathrm{th}}^{\text{“0”}})$, where $V_{\mathrm{th}}^{\text{“1”}}$ and $V_{\mathrm{th}}^{\text{“0”}}$ are the threshold voltage of the device in the "1" and in the "0" states, respectively. Recall that to obtain this modulation of the photodoping we do laser exposures of 20 s together with gate voltage applications. The generated photodoping with a 20 s laser exposure is an order of magnitude lower than the maximum photodoping ($\Delta n_{\mathrm{ph}} \sim 10^{13}\,\mathrm{cm}^{-2}$) obtained in this work, see Fig. 1(d), where the photodoping is maximized by waiting for the saturation of the photocurrent after 30 min laser exposure. Such high photodoping modulation give an ultra-high memory on/off ratio of 10^6 in Fig. 1(e). However, we can still obtain a high memory on/off ratio of 10^4 by using laser exposures of 20 s, see Fig. S14.

Finally, we discuss the process of photodoping that possibly generates the PPC and the photomemory effect in our MoS_2 FETs. It is important to mention that the PPC is not a consensus topic. The most discussed explanations for the PPC in MoS_2 is either due to the photo-induced charge transfer from adsorbed gases to the MoS_2 channel [33] or due to the Coulomb interaction with defects at the insulator surface [20–22, 32, 34–37]. We believe that the interactions with adsorbed gases are not a valid explanation in our devices as there is no hysteresis in the σ vs V_{BG} curves when we sweep the voltage in opposite directions [38](see Fig. S7). We believe that the interactions with defects at the insulator surface are not the dominant mechanism, as the devices have a low density of defects when compared with the photodoping observed in our work ($10^{13}\,\mathrm{cm}^{-2}$). Furthermore, the fact that we measure the photodoping in a clean and flat BN substrate [39] reinforces this statement.
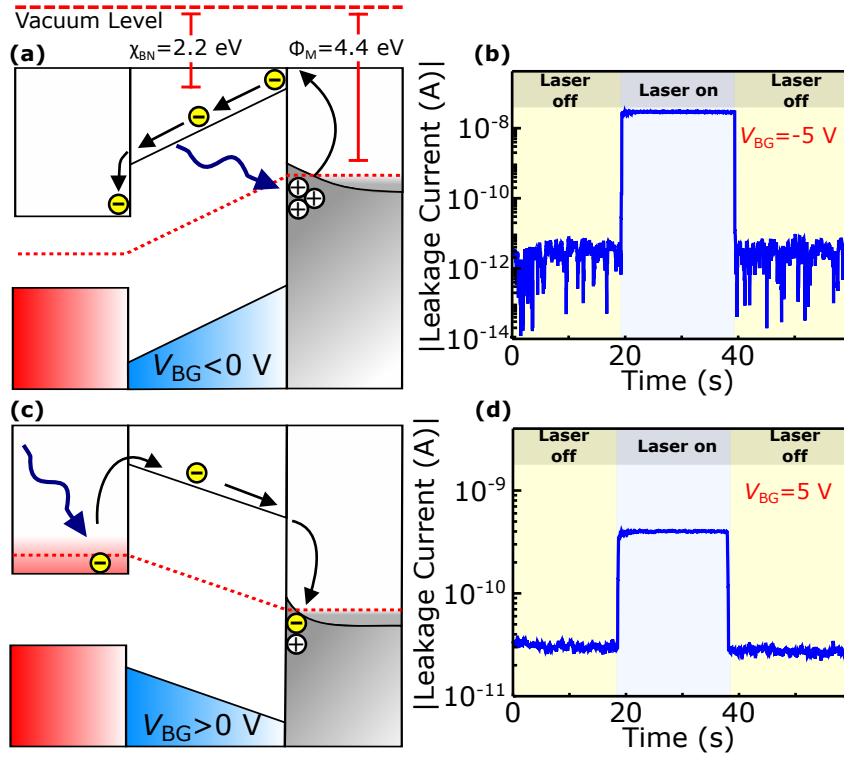
FIG. 3. **Physical model for the photodoping**. **(a)**, energy band diagram for the MoS$_2$/BN/graphite junction as a function of position for $V_{BG} < 0$ V. **(b)**, photogenerated leakage current, $V_{BG} = -5$ V, $\lambda = 488$ nm and fluence of 60 μW/μm^2. **(c)**, energy band diagram for the MoS$_2$/BN/graphite junction as a function of position for $V_{BG} > 0$ V. **(d)**, photogenerated leakage current, $V_{BG} = 5$ V, $\lambda = 488$ nm and fluence of 60 μW/μm^2.

Consider that we use a ~ 30 nm thick BN, which prevents tunneling as a charge-trapping mechanim like occurs in the reference [15–17]. It should be also mentioned that to prepare our Van der Waals heteroestructures we use the same wet-transfer method of the reference [39], which leaves some bubbles and wrinkles between the BN and the graphite flakes, see Fig. S1 and Fig. S2. However, in spite of these issues, the BN is clean and atomically flat in the majority of the surface of the devices. Recall that we do not study the influence of these imperfections between the layers in the photodoping effect, but we do not discard that they can play a role.

Thus, we shall attribute a different process to the photodoping in our MoS$_2$ FET, which we propose to be a photogeneration of trapped holes in the gate-insulator interface. We clarify this mechanism by drawing the energy band diagram of the MoS$_2$ FET. Fig. 3(a)

shows a band diagram of the MoS$_2$ FET with $V_{\mathrm{BG}} < 0$ V applied to the graphite relative to the MoS$_2$. Here $\chi_{\mathrm{MoS_2}}$ is the MoS$_2$ electron affinity, χ_{BN} is the BN electron affinity and Φ_{M} is the graphite work function. We also show in the gate-insulator junction the bending of the graphite band, that generates a built-in electric field. For $V_{\mathrm{BG}} < 0$ V, photons with sufficient energy ($E_{\mathrm{L}} > \Phi_{\mathrm{M}} - \chi_{\mathrm{BN}}$) promote the electrons from the gate-insulator interface to the conduction band of BN. The applied negative gate voltage drives these photoexcited electrons through the conduction band of BN to the MoS$_2$ channel, but some holes generated during the photoabsorption process remain trapped at the gate-insulator interface by the electric field of the gate-insulator junction. The positively charged layer generates photodoping in the MoS$_2$ channel, see Fig. 3(a). According to this energy diagram description, we predict that we should observe a photo-generated leakage current under laser exposure between the drain and gate electrodes. This fact is verified in our experiments, as depicted in Fig. 3(b) that exhibits a 10^{-8} A leakage current during the laser exposure.

For $V_{\mathrm{BG}} > 0$ V, the MoS$_2$ channel is n-doped, so when we turn the laser on, the electrons from MoS$_2$ are photoexcited to the conduction band of BN, see Fig. 3(c). In this case, the gate-field drives these electrons through the conduction band of BN to the gate-insulator junction, recombining with some of the trapped holes, reducing the photodoping. We do not achieve the photodoping reduction process totally, because the built-in electric field of the gate-insulator junction prevents some of the electrons to recombine. Fig. 3(d) shows that for $V_{\mathrm{BG}} > 0$ V we can also observe a photo-generated leakage current during the laser exposure. Note that for $V_{\mathrm{BG}} > 0$ V the photo-generated leakage current is lower than for $V_{\mathrm{BG}} < 0$ V. We can associate this fact to the density of states of MoS$_2$, which is smaller than the graphite flake. It is also important to mention that this asymmetry in the photo-generated leakage current imposes a faster "write" operation relative to the "erase" operation, see Fig. S10.

The proposed model in Fig. 3 explains the results of Fig. 2(b), which shows that the applied negative gate bias increase the photodoping, whether positive gate bias reduce the photodoping. Moreover, the threshold energy for photodoping generation ($E_{\mathrm{th}} = \Phi_{\mathrm{M}} - \chi_{\mathrm{BN}}$) in Fig. 3 matches our experimental results. Indeed, a crystal of BN possess a band gap ($E_{\mathrm{g}}^{\mathrm{BN}}$) of 5.2-5.9 eV and electron affinity (χ_{BN}) of 2.0-2.3 eV [1]. Whereas graphite has a work function (Φ_{G}) of 4.3-4.6 eV [40–42]. Therefore, the difference between Φ_{G} and χ_{BN} is around 2.2 eV, so only photons with energy larger than 2.2 eV are predicted to promote photoexcitation, see Fig. 3(a). Therefore, we have done measurements with a laser energy

of 1.6 eV and measured an almost negligible photodoping of $\Delta n_\mathrm{ph} \sim 10^{10}\,\mathrm{cm}^{-2}$ (see Fig. S11). In contrast, for the laser energy of 2.5 eV we have observed a high photodoping of $\Delta n_\mathrm{ph} \sim 10^{12}\,\mathrm{cm}^{-2}$ (see Fig. S13). The small, but not null, photodoping with the 1.6 eV laser may be due to other minor effects that may also occur, as the excitation of defects from the MoS_2 channel [43]. However, mostly the gate-insulator interface contains the physics of the photodoping, therefore studying other materials may enable photomemory improvements.

Conclusion

In conclusion, we have demonstrated that it is possible to obtain a non-volatile photomemory effect with high on/off ratio in a FET architecture. We showed that high values of doping are achieved via laser exposure that generates the binary photomemory states with high on/off ratio. We have shown that the photomemory described presents long memory retention time and thus the photomemory states are non-volatile. We have also verified that the photomemory states can be controlled and adjusted by the applied gate voltage, that could also be used to improve the memory on/off ratio. Finally, we have proposed a phenomenological model that agrees well with the experimental observations and clarifies a possible nature of the photodoping effect in MoS_2 FETs. Our results widen the possibilities of memory applications using 2D materials.

METHODS

Device Fabrication. The devices are obtained by transfer [39] of BN crystals ($\sim 30\,\mathrm{nm}$ thick) to graphite crystals ($\sim 20\,\mathrm{nm}$ thick). Metal leads were patterned by electron-beam lithography and subsequent deposition of metals (Cr 1 nm/ Au 50 nm). Monolayer MoS_2 flakes were transferred to this structure by dry viscoelastic stamping technique [44]. For more details see Supplementary Information.

Optoelectronic Measurements. To provide a source-drain bias the external DC source of a standard lock-in amplifier (SR830) was used. While to provide a gate bias the DC source of the lock-in amplifier or a Keithley 2400 were used. The current of the devices was collected by a pre-amplifier and then measured by a multimeter (Keithley 2000). To generate the photocurrent in the MoS_2 FET a 488 nm laser beam was focused in the devices

by a $50\times$ objective lens ($\sim 1\,\mu$m spotsize).

REFERENCES

[1] Min Sup Choi, Gwan-Hyoung Lee, Young-Jun Yu, Dae-Yeong Lee, Seung Hwan Lee, Philip Kim, James Hone, and Won Jong Yoo. Controlled charge trapping by molybdenum disulphide and graphene in ultrathin heterostructured memory devices. *Nature Communications*, 4:1624–, March 2013.

[2] Enze Zhang, Weiyi Wang, Cheng Zhang, Yibo Jin, Guodong Zhu, Qingqing Sun, David Wei Zhang, Peng Zhou, and Faxian Xiu. Tunable charge-trap memory based on few-layer MoS_2. *ACS Nano*, 9(1):612–619, 2015. PMID: 25496773.

[3] Simone Bertolazzi, Daria Krasnozhon, and Andras Kis. Nonvolatile memory cells based on MoS_2/graphene heterostructures. *ACS Nano*, 7(4):3246–3252, 2013. PMID: 23510133.

[4] Myung Hun Woo, Byung Chul Jang, Junhwan Choi, Khang June Lee, Gwang Hyuk Shin, Hyejeong Seong, Sung Gap Im, and Sung-Yool Choi. Low-power nonvolatile charge storage memory based on MoS_2 and an ultrathin polymer tunneling dielectric. *Advanced Functional Materials*, pages 1703545–n/a. 1703545.

[5] Juwon Lee, Sangyeon Pak, Young-Woo Lee, Yuljae Cho, John Hong, Paul Giraud, Hyeon Suk Shin, Stephen M. Morris, Jung Inn Sohn, SeungNam Cha, and Jong Min Kim. Monolayer optical memory cells based on artificial trap-mediated charge storage and release. *Nature Communications*, 8:14734–, March 2017.

[6] G. He, H. Ramamoorthy, C.-P. Kwan, Y.-H. Lee, J. Nathawat, R. Somphonsane, M. Matsunaga, A. Higuchi, T. Yamanaka, N. Aoki, Y. Gong, X. Zhang, R. Vajtai, P. M. Ajayan, and J. P. Bird. Thermally assisted nonvolatile memory in monolayer MoS_2 transistors. *Nano Letters*, 16(10):6445–6451, 2016. PMID: 27680095.

[7] Gwang Hyuk Shin, Choong-Ki Kim, Gyeong Sook Bang, Jong Yun Kim, Byung Chul Jang, Beom Jun Koo, Myung Hun Woo, Yang-Kyu Choi, and Sung-Yool Choi. Multilevel resistive switching nonvolatile memory based on MoS_2 nanosheet-embedded graphene oxide. *2D Materials*, 3(3):034002, 2016.

[8] Augustin J. Hong, Emil B. Song, Hyung Suk Yu, Matthew J. Allen, Jiyoung Kim, Jesse D. Fowler, Jonathan K. Wassei, Youngju Park, Yong Wang, Jin Zou, Richard B. Kaner, Bruce H. Weiller, and Kang L. Wang. Graphene flash memory. *ACS Nano*, 5(10):7812–7817, 2011. PMID: 21854056.

[9] Yi Zheng, Guang-Xin Ni, Chee-Tat Toh, Ming-Gang Zeng, Shu-Ting Chen, Kui Yao, and Barbaros Őzyilmaz. Gate-controlled nonvolatile graphene-ferroelectric memory. *Applied Physics Letters*, 94(16):163505, 2009.

[10] Brian Standley, Wenzhong Bao, Hang Zhang, Jehoshua Bruck, Chun Ning Lau, and Marc Bockrath. Graphene-based atomic-scale switches. *Nano Letters*, 8(10):3345–3349, 2008. PMID: 18729415.

[11] Xiaomu Wang, Weiguang Xie, Jun Du, Chengliang Wang, Ni Zhao, and Jian-Bin Xu. Graphene/metal contacts: Bistable states and novel memory devices. *Advanced Materials*, 24(19):2614–2619, 2012.

[12] Congli He, Zhiwen Shi, Lianchang Zhang, Wei Yang, Rong Yang, Dongxia Shi, and Guangyu Zhang. Multilevel resistive switching in planar graphene/SiO$_2$ nanogap structures. *ACS Nano*, 6(5):4214–4221, 2012. PMID: 22519726.

[13] Xiao-Dong Zhuang, Yu Chen, Gang Liu, Pei-Pei Li, Chun-Xiang Zhu, En-Tang Kang, Koon-Gee Noeh, Bin Zhang, Jin-Hui Zhu, and Yong-Xi Li. Conjugated-polymer-functionalized graphene oxide: Synthesis and nonvolatile rewritable memory effect. *Advanced Materials*, 22(15):gropo, 2010.

[14] Dong Li, Mingyuan Chen, Zhengzong Sun, Peng Yu, Zheng Liu, Pulickel M. Ajayan, and Zengxing Zhang. Two-dimensional non-volatile programmable p-n junctions. *Nature Nanotechnology*, 12:901–, June 2017.

[15] Quoc An Vu, Yong Seon Shin, Young Rae Kim, Van Luan Nguyen, Won Tae Kang, Hyun Kim, Dinh Hoa Luong, Il Min Lee, Kiyoung Lee, Dong-Su Ko, Jinseong Heo, Seongjun Park, Young Hee Lee, and Woo Jong Yu. Two-terminal floating-gate memory with van der waals heterostructures for ultrahigh on/off ratio. *Nature Communications*, 7:12725–, September 2016.

[16] Ruiqing Cheng, Feng Wang, Lei Yin, Kai Xu, Tofik Ahmed Shifa, Yao Wen, Xueying Zhan, Jie Li, Chao Jiang, Zhenxing Wang, and Jun He. Multifunctional tunneling devices based on graphene/h-bn/mose2 van der waals heterostructures. *Applied Physics Letters*, 110(17):173507, 2017.

[17] Yu Wang, Erfu Liu, Anyuan Gao, Tianjun Cao, Mingsheng Long, Chen Pan, Lili Zhang, Junwen Zeng, Chenyu Wang, Weida Hu, Shi-Jun Liang, and Feng Miao. Negative photoconductance in van der waals heterostructure-based floating gate phototransistor. *ACS Nano*, 12(9):9513–9520, September 2018.

[18] B. Radisavljevic, A. Radenovic, J. Brivio, V. Giacometti, and A. Kism. Single-layer MoS_2 transistors. *Nat Nano*, 6(3):147–150, March 2011.

[19] Sajedeh Manzeli, Dmitry Ovchinnikov, Diego Pasquier, Oleg V. Yazyev, and Andras Kis. 2d transition metal dichalcogenides. *Nature Reviews Materials*, 2:17033–, June 2017.

[20] Oriol Lopez-Sanchez, Dominik Lembke, Metin Kayci, Aleksandra Radenovic, and Andras Kis. Ultrasensitive photodetectors based on monolayer MoS_2. *Nat Nano*, 8(7):497–501, July 2013.

[21] M. F. Khan, M. W. Iqbal, M. Z. Iqbal, M. A. Shehzad, Y. Seo, and Jonghwa Eom. Photocurrent response of MoS_2 field-effect transistor by deep ultraviolet light in atmospheric and N_2 gas environments. *ACS Applied Materials & Interfaces*, 6(23):21645–21651, 2014. PMID: 25409490.

[22] Wenjing Zhang, Jing-Kai Huang, Chang-Hsiao Chen, Yung-Huang Chang, Yuh-Jen Cheng, and Lain-Jong Li. High-gain phototransistors based on a cvd MoS_2 monolayer. *Advanced Materials*, 25(25):3456–3461, 2013.

[23] Zongyou Yin, Hai Li, Hong Li, Lin Jiang, Yumeng Shi, Yinghui Sun, Gang Lu, Qing Zhang, Xiaodong Chen, and Hua Zhang. Single-layer MoS_2 phototransistors. *ACS Nano*, 6(1):74–80, 2012. PMID: 22165908.

[24] Woong Choi, Mi Yeon Cho, Aniruddha Konar, Jong Hak Lee, Gi-Beom Cha, Soon Cheol Hong, Sangsig Kim, Jeongyong Kim, Debdeep Jena, Jinsoo Joo, and Sunkook Kim. High-detectivity multilayer MoS_2 phototransistors with spectral response from ultraviolet to infrared. *Advanced Materials*, 24(43):5832–5836, 2012.

[25] Riccardo Frisenda, Aday J. Molina-Mendoza, Thomas Mueller, Andres Castellanos-Gomez, and Herre S. J. van der Zant. Atomically thin p-n junctions based on two-dimensional materials. *Chem. Soc. Rev.*, 47(9):3339–3358, 2018.

[26] Kin Fai Mak, Changgu Lee, James Hone, Jie Shan, and Tony F. Heinz. Atomically thin MoS_2: A new direct-gap semiconductor. *Phys. Rev. Lett.*, 105:136805, Sep 2010.

[27] Andrea Splendiani, Liang Sun, Yuanbo Zhang, Tianshu Li, Jonghwan Kim, Chi-Yung Chim, Giulia Galli, and Feng Wang. Emerging photoluminescence in monolayer MoS_2. *Nano Letters*, 10(4):1271–1275, 2010. PMID: 20229981.

[28] Hualing Zeng, Junfeng Dai, Wang Yao, Di Xiao, and Xiaodong Cui. Valley polarization in MoS$_2$ monolayers by optical pumping. *Nat Nano*, 7(8):490–493, August 2012.

[29] Kin Fai Mak, Keliang He, Jie Shan, and Tony F. Heinz. Control of valley polarization in monolayer MoS$_2$ by optical helicity. *Nat Nano*, 7(8):494–498, August 2012.

[30] Ting Cao, Gang Wang, Wenpeng Han, Huiqi Ye, Chuanrui Zhu, Junren Shi, Qian Niu, Pingheng Tan, Enge Wang, Baoli Liu, and Ji Feng. Valley-selective circular dichroism of monolayer molybdenum disulphide. *Nat Commun*, 3:887–, June 2012.

[31] K. F. Mak, K. L. McGill, J. Park, and P. L. McEuen. The valley hall effect in MoS$_2$ transistors. *Science*, 344(6191):1489–1492, 2014.

[32] Ju L., J. Velasco Jr, Huang E., Kahn S., Nosiglia C., Hsin-Zon Tsai, Yang W., Taniguchi T., Watanabe K., Zhang Y., Zhang G., Crommie M., Zettl A., and Wang F. Photoinduced doping in heterostructures of graphene and boron nitride. *Nat Nano*, 9(5):348–352, May 2014.

[33] Bastian Miller, Eric Parzinger, Anna Vernickel, Alexander W. Holleitner, and Ursula Wurstbauer. Photogating of mono- and few-layer MoS$_2$. *Applied Physics Letters*, 106(12):122103, 2015.

[34] Marco M. Furchi, Dmitry K. Polyushkin, Andreas Pospischil, and Thomas Mueller. Mechanisms of photoconductivity in atomically thin MoS$_2$. *Nano Letters*, 14(11):6165–6170, 2014. PMID: 25299515.

[35] Yueh-Chun Wu, Cheng-Hua Liu, Shao-Yu Chen, Fu-Yu Shih, Po-Hsun Ho, Chun-Wei Chen, Chi-Te Liang, and Wei-Hua Wang. Extrinsic origin of persistent photoconductivity in monolayer MoS$_2$ field effect transistors. *Scientific Reports*, 5:11472–, June 2015.

[36] Young Duck Kim, Myung-Ho Bae, Jung-Tak Seo, Yong Seung Kim, Hakseong Kim, Jae Hong Lee, Joung Real Ahn, Sang Wook Lee, Seung-Hyun Chun, and Yun Daniel Park. Focused-laser-enabled p-n junctions in graphene field-effect transistors. *ACS Nano*, 7(7):5850–5857, 2013. PMID: 23782162.

[37] Antonio Di Bartolomeo, Luca Genovese, Tobias Foller, Filippo Giubileo, Giuseppe Luongo, Luca Croin, Shi-Jun Liang, L K Ang, and Marika Schleberger. Electrical transport and persistent photoconductivity in monolayer MoS$_2$ phototransistors. *Nanotechnology*, 28(21):214002, 2017.

[38] Dattatray J. Late, Bin Liu, H. S. S. Ramakrishna Matte, Vinayak P. Dravid, and C. N. R. Rao. Hysteresis in single-layer MoS$_2$ field effect transistors. *ACS Nano*, 6(6):5635–5641, 2012.

PMID: 22577885.

[39] Dean C. R., Young A. F., MericI., Lee C., Wang L., Sorgenfrei S., Watanabe K., Taniguchi T., Kim P., Shepard K. L., and Hone J. Boron nitride substrates for high-quality graphene electronics. *Nat Nano*, 5(10):722–726, October 2010.

[40] K. S. KRISHNAN and S. C. JAIN. Thermionic constants of graphite. *Nature*, 169(4304):702–703, April 1952.

[41] Yingke Zhou, Timothy Holme, Joe Berry, Timothy R. Ohno, David Ginley, and Ryan O'Hayre. Dopant-induced electronic structure modification of hopg surfaces: Implications for high activity fuel cell catalysts. *The Journal of Physical Chemistry C*, 114(1):506–515, 2010.

[42] Keishi Akada, Tomo o Terasawa, Gaku Imamura, Seiji Obata, and Koichiro Saiki. Control of work function of graphene by plasma assisted nitrogen doping. *Applied Physics Letters*, 104(13):131602, 2014.

[43] Péter Vancsó, Gábor Zsolt Magda, János Peto, Ji-Young Noh, Yong-Sung Kim, Chanyong Hwang, László P. Biró, and Levente Tapasztó. The intrinsic defect structure of exfoliated mos2 single layers revealed by scanning tunneling microscopy. *Scientific Reports*, 6:29726–, July 2016.

[44] Andres Castellanos-Gomez, Michele Buscema, Rianda Molenaar, Vibhor Singh, Laurens Janssen, Herre S J van der Zant, and Gary A Steele. Deterministic transfer of two-dimensional materials by all-dry viscoelastic stamping. *2D Materials*, 1(1):011002, 2014.

Acknowledgments

Competing Financial Interests

The authors declare no competing financial interests